Melt Rheology of Polypropylene Reinforced with Polyaniline-Coated Short Glass Fibers

María Eugenia Romero-Guzmán,[1] Angel Romo-Uribe,[1] Agustín E. González,[1] Rodolfo Cruz-Silva[2]

[1]*Laboratorio de Nanopolímeros y Coloides, Instituto de Ciencias Físicas, Universidad Nacional Autónoma de México, Av. Universidad s/n, Col. Chamilpa, CP 62210, Cuernavaca, Morelos, México*
[2]*Centro de Investigación en Ingeniería y Ciencias Aplicadas, UAEM., Av. Universidad 1001, Col. Chamilpa, CP 62210, Cuernavaca, Morelos, México*

Received 10 October 2007; accepted 1 February 2008
DOI 10.1002/app.28333
Published online 2 May 2008 in Wiley InterScience (www.interscience.wiley.com).

ABSTRACT: This research deals with the melt rheology of isotactic polypropylene (iPP) reinforced with short glass fibers (SGF) coated with electrically conductive polyaniline (PAn). Composites containing 10, 20, and 30 wt % PAn-SGF were studied. Moreover, a composite of 30 wt % PAn-SGF was also prepared with a blend of iPP and PP-grafted-maleic anhydride (iPP/PP-gMA). The composites showed linear viscoelastic regime at small strain amplitudes. The onset of nonlinearity decreased as the concentration of filler increased. The time-temperature superposition principle applied to all composites. The filler increased the shear moduli (G', G'') and the complex viscosity η^*. Steady-state shear experiments showed yield stress for the composites with 20 and 30 wt % PAn-SGF. Strikingly, the 10 wt % composite showed higher steady state viscosity than the 20 wt %. Rheo-optics showed that shear induced disorder of microfibers at a concentration of 10 wt %. However, at 20 wt % concentration shear aligned the microfibers along the flow axis, this would explain the anomalous steady state viscosity values. The viscosity exhibited a shear thinning behavior at high shear rates for all composites. Creep experiments showed that the filler induced greater strain recovery in the composites and that the amount of strain recovery increased as the PAn-SGF concentration increased. However, the enhancement of strain recovery (as well as shear viscosity) was more significant when using the iPP/PP-gMA blend, suggesting greater adhesion between this matrix and the filler PAn-SGF. © 2008 Wiley Periodicals, Inc. J Appl Polym Sci 109: 2207–2218, 2008

Key words: composites; rheology; polypropylene; electrically conductive composites

INTRODUCTION

In recent years reinforced polymer composites have been intensively investigated in both industrial and academic fields, because they exhibit valuable mechanical and thermal properties when compared with their neat counterparts. This is the case of polypropylene (PP), which is widely used in many applications because of its low production cost and versatile properties. There are many studies concerned with the improvement of mechanical properties of PP. For instance, the addition of elastomer particles, such as SEBS improves the impact resistance but significantly reduces the stiffness and yield strength.[1–4] Improvement in impact resistance of PP was also obtained with the addition of calcium carbonate ($CaCO_3$).[5] Adding glass fibers to PP is a relatively easy and effective method for enhancing tensile, flexural and impact properties.[6–8] Several investigators have carried out experimental studies[6–11] and developed theoretical models[12–14] on glass fiber-reinforced PP.

The tremendous growth in aerospace, defense and automotive industries has resulted in the development of new reinforced-polymer composites with new properties. In this study we utilized a novel electrically conductive reinforced composite, polypropylene (iPP) reinforced with short glass fibers (SGF). The SGF were coated with electrically conducting polyaniline (PAn) by *in situ* polymerization.[15,16]

Polyaniline, an intrinsically conductive polymer, has been increasingly employed in the preparation of thermoplastics-based composites for electromagnetic shielding or antistatic applications.[17–23] The great potential of this polymer in the aforesaid applications is due to its environmental stability, relatively high electrical conductivity and low-cost synthetic route.[24] However, the addition of PAn to polymer matrices usually results in a loss or degradation of mechanical properties, compromising the performance of these composites. To combine the electrical conductivity of PAn and the reinforcing properties of glass fibers synthetic routes have been developed where SGFs are coated with PAn.[16,25] The

Correspondence to: A. Romo-Uribe (aromo-uribe@fis.unam.mx).

PAn-coated-SGF (PAn-SGF) are then easily added to a polymer matrix, for instance, by extrusion processing. The synthetic route, and the mechanical, thermal and electrical properties of iPP/PAn-SGF composites have been investigated by Cruz-Silva et al.[15,16] The PAn-SGF, with a surface conductivity of 3.3×10^{-1} S/cm, increments the Young's modulus of the composites. The incorporation of small amount of PP-maleic anhydride copolymer (PP-gMA) to the composites also improved their mechanical properties, but affected negatively the electrical conductivity of the composites due, apparently, to fiber encapsulation.[16]

The aim of this work was to investigate the effect of the PAn-coated-SGF on the rheological properties of two matrix materials, neat iPP and iPP/PP-gMA polymer blend. Our results will show that PAn-SGF incorporation into iPP modifies the rheological propierties, increasing and then decreasing the melt viscosity of the composites. On the other hand, the addition of a small amount of PP-gMA resulted in a significant increase in melt viscosity and recoverable strain. These results suggest better interaction between the blend iPP/PP-gMA and the filler PAn-SGF. The overall rheological properties depend strongly on the concentration of the reinforcing material. Finally, there appears to be an influence of the orientation of the fibers on the steady shear viscosity.

EXPERIMENTAL

Materials

The preparation of the PAn-SGF and the iPP/PAn-SGF electrically conducting composites have been described in detail elsewhere.[15,16] PAn-SGF was thermally blended with isotactic polypropylene homopolymer (*Valtec HP423M*, MFI 3.8, density 0.9 g/cm^3) in a batch mixer (*Brabender Plasticorder PL2000*) at 60 rpm for 12 min at 200°C. Polymer composites with concentrations of PAn-SGF ranging from 10 to 30 wt % were prepared. The resulting composites were compression molded into plaques of 2.6 mm thickness at 200°C under a load of 2.45 MPa for 10 min. Two different sorts of composites were investigated, iPP/PAn-SGF and iPP/PP-gMA/PAn-SGF, where PP-gMA is a PP-maleic anhydride copolymer. Table I shows the compositions of the PAn-SGF composites. Fiber length for all the composites was determined before carrying out the rheological characterization. The composites were placed on the observation stage and images were captured using a digital camera (Moticam 350, manufactured by Motic), and coupled to a Leitz optical microscope. The image analysis software Image Tool v 3.0 (UTHSCSA) was used to characterize the length of the fibers.

TABLE I
Composition of the PAn-SGF Composites (wt %)

Sample	iPP	PP-gMA	PAn-coated SGF
PP0000	100	0	0
PP0010	90	0	10
PP0020	80	0	20
PP0030	70	0	30
PP0530	65	5	30
PP-gMA	0	100	0

Rheological characterization

The rheological properties of the composites were studied with a stress-controlled CVO Rheometer manufactured by Malvern Instruments. The rheometer was equipped with 25 mm diameter parallel plates, and a gap of 1 mm was utilized throughout. The existence and extent of the linear viscoelastic (LVE) regime was determined measuring the dynamic storage and loss moduli, $G'(\omega)$ and $G''(\omega)$, as a function of strain, γ, at 1 Hz. The dynamic rheological measurements were carried out from 190 to 230°C. The temperature control was better than ± 0.2°C. The experimental protocol was as follows: the rheometer was heated to 190°C, allowed to equilibrate and the gap separation set. Fresh samples were loaded in the preheated rheometer, holding for 15 min to allow for thermal equilibrium before measurements started. The shear viscosity as a function of shear rate was determined by operating the rheometer in the viscometry mode at constant temperature of 190°C. The upper shear rate range was limited up to 10 s^{-1} because of flow instabilities in the gap between the plates, which causes melt fracture. Creep recovery measurements were conducted by operating the rheometer at controlled stress and at temperature of 190°C. The applied shear stress was 10 Pa and the resultant deformation was measured as a function of time and applied stress. After applying shear stress for periods of 10, 20, 50, and 100 s, the strain recovery was monitored for 300 s.

Rheo-optics

In situ microscopic observations of the composites under steady shear were carried out at 190°C using a hot-stage and controller FP-90 manufactured by Mettler. A thin sample of about 40 μm thickness was placed between two glass slides. Shear was applied by sliding the upper slide, while maintaining the lower plate static, using the screw attached to the hot stage built-in traversing stage. Following the procedure reported by other researchers,[26–28] the average shear rate was determined from the known sample thickness and recording the distance traversed and the associated time elapsed. Despite the simplic-

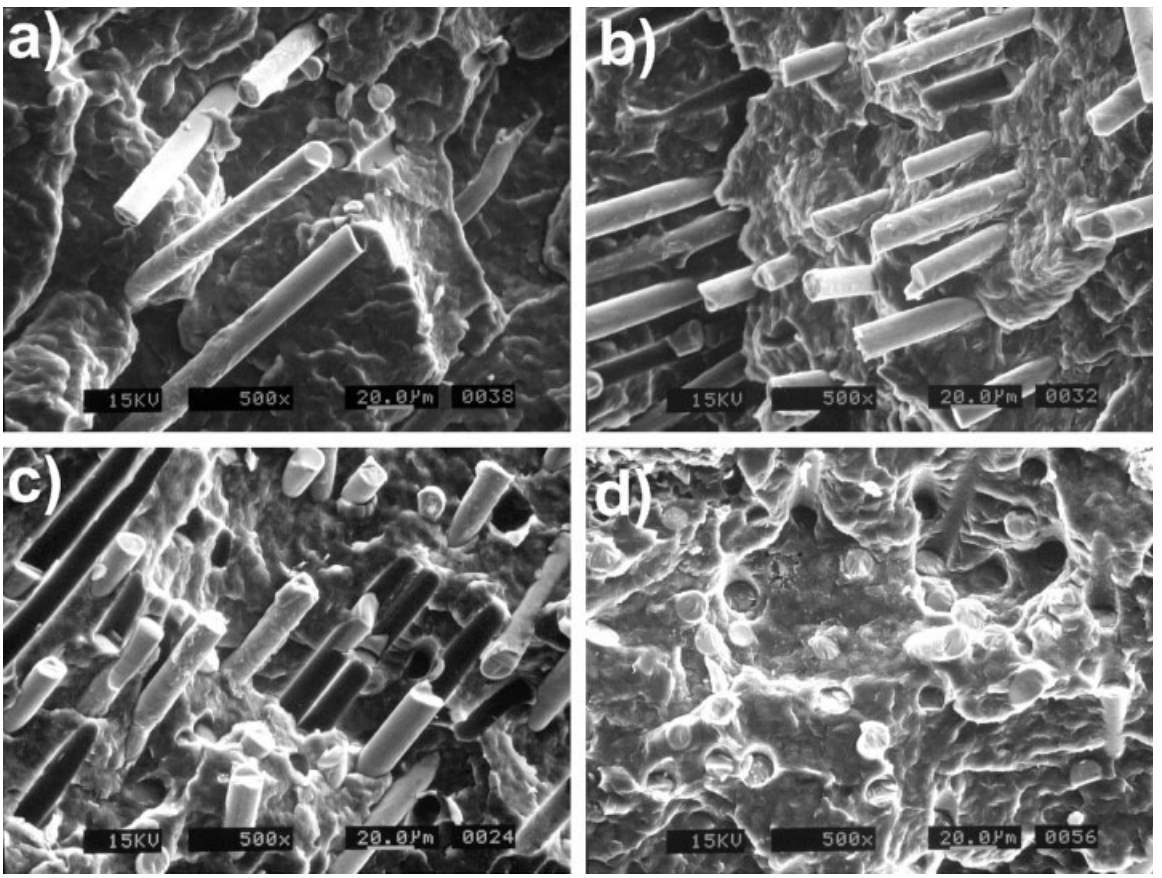

Figure 1 Scanning electron micrographs of isotactic popypropylene, iPP reinforced with PAn-coated short glass fibers (SGF): (a) 10, (b) 20, and (c) 30 wt % filler concentration. (d) SEM micrograph of iPP/PP-gMA blend reinforced with 30 wt % PAn-SGF.

ity of this approach, it was found that a slow velocity of 0.02 mm/s could be reproduced within 20%. This translated into an average shear rate of 0.5 s^{-1}, which is within the range of interest, as discussed in the Results section. The sheared sample was imaged using white light conditions and the micrographs were digitally captured using the Moticam 350 camera (Motic).

Scanning electron microscopy

The fracture morphology of polyaniline coated short glass fibers was observed in a TopCom 510 scanning electron microscope. Composite samples were fractured under liquid nitrogen, and coated with a thin layer of Au/Pd before observation.

RESULTS AND DISCUSSION

Morphology

Figure 1 shows SEM micrographs of the freeze-fractured composites. Figure 1(a-c) show the iPP composites with 10, 20, and 30 wt % of PAn-SGF, respectively. The fracture in all cases occurs by pull-out of the fibers because of the low interfacial adhesion between the surface of the fibers and the polymer matrix, in agreement with previous results from our group[16] and others.[20] In addition, Figure 1(c) shows several side-by-side fibers, which indicate that at 30 wt % concentration the fibers start to aggregate, increasing the electrical conductivity of the composite by a percolation process.[16] On the other hand, Figure 1(d) shows the fracture surface of the composite with 30 wt % of PAn-SGF and 5% of the PP-gMA, which now involves extensive fiber breakage, suggesting an increment in interfacial adhesion. At the same time, dispersion of the fiber within the iPP/PP-gMA matrix has improved and the image shows only isolated PAn-SGF. The dramatic change in interfacial adhesion and dispersion of the fibers has an effect on the rheological properties, as will be discussed below.

Fiber breakage takes place during the processing of short fiber-reinforced composites materials. Length of fibers in the composites is one of the major factors influencing the ultimate properties of the composite materials in addition of fiber content, fiber–matrix interaction, extent of intermingling of different types of fibers, orientation of the fibers and

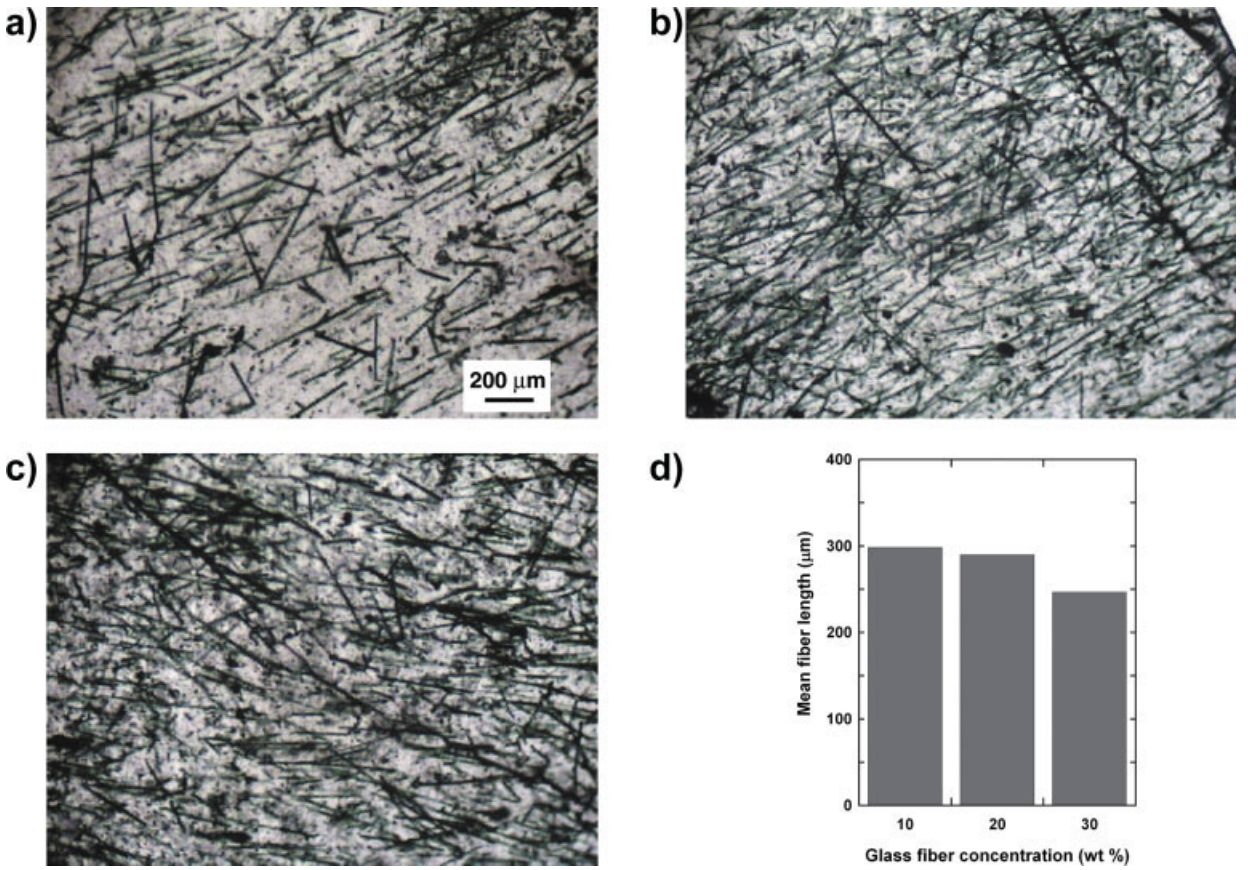

Figure 2 iPP/PAn-SGF composites viewed under the optical microscope: (a) 10, (b) 20, and (c) 30 wt % fibers. (d) Number-average glass fiber length as a function of filler concentration. [Color figure can be viewed in the online issue, which is available at www.interscience.wiley.com.]

hybrid design.[7] Figure 2(a-c) shows micrographs of 50-μm-thick samples as a function of PAn-SGF concentration. The fiber length distribution of each composite was evaluated from these images by measuring the length of individual fibers (at least 50 for each composite). The effect of glass fiber length as a function of concentration in the composites is summarized in Figure 2(d). It is noted that the glass fiber lengths decrease slightly with the increase of glass fiber concentration in the composites, with an average length of 298, 290, and 247 μm, for 10, 20, and 30 wt % of PAn-SGF, respectively. The length standard deviation was found to be within 20%. The SEM analysis showed that the coated glass fibers had an average diameter of 14 μm,[15,16] thus the average aspect ratio for the fibers was $L/D \approx 21.3$, 20.7, and 17.6. The reduction of glass fiber length with the increase of glass fiber concentration was also observed for polypropylene with 5 and 20 wt % of long glass fibers,[9] and in a hemp/glass/PP hybrid composite.[7]

Small strain oscillatory shear

Investigation of the linear viscoelastic behavior was carried out by applying strain sweeps at controlled frequency of 1 Hz. Figure 3 shows the storage modulus, G', as a function of strain, γ. We can see that iPP and its composites are linearly viscoelastic (LVE) up to about 0.01% strain. Therefore, the dynamic

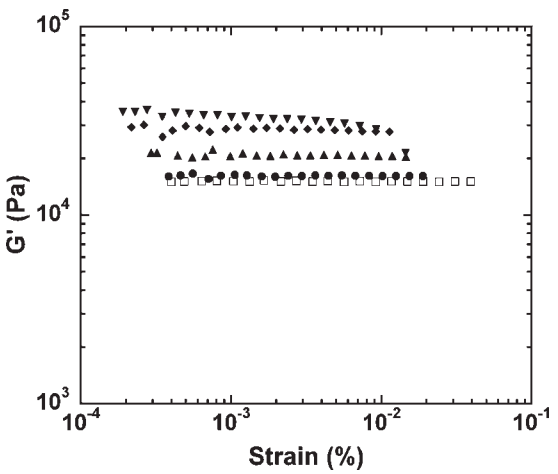

Figure 3 Storage modulus, G', for iPP containing: 0 (□), 10 (●), 20 (▲) and 30 (▼) wt % PAn-SGF; and iPP/PP-gMA with 30 wt % PAn-SGF (◆). Strain sweep experiment at frequency of 1 Hz, at 190°C.

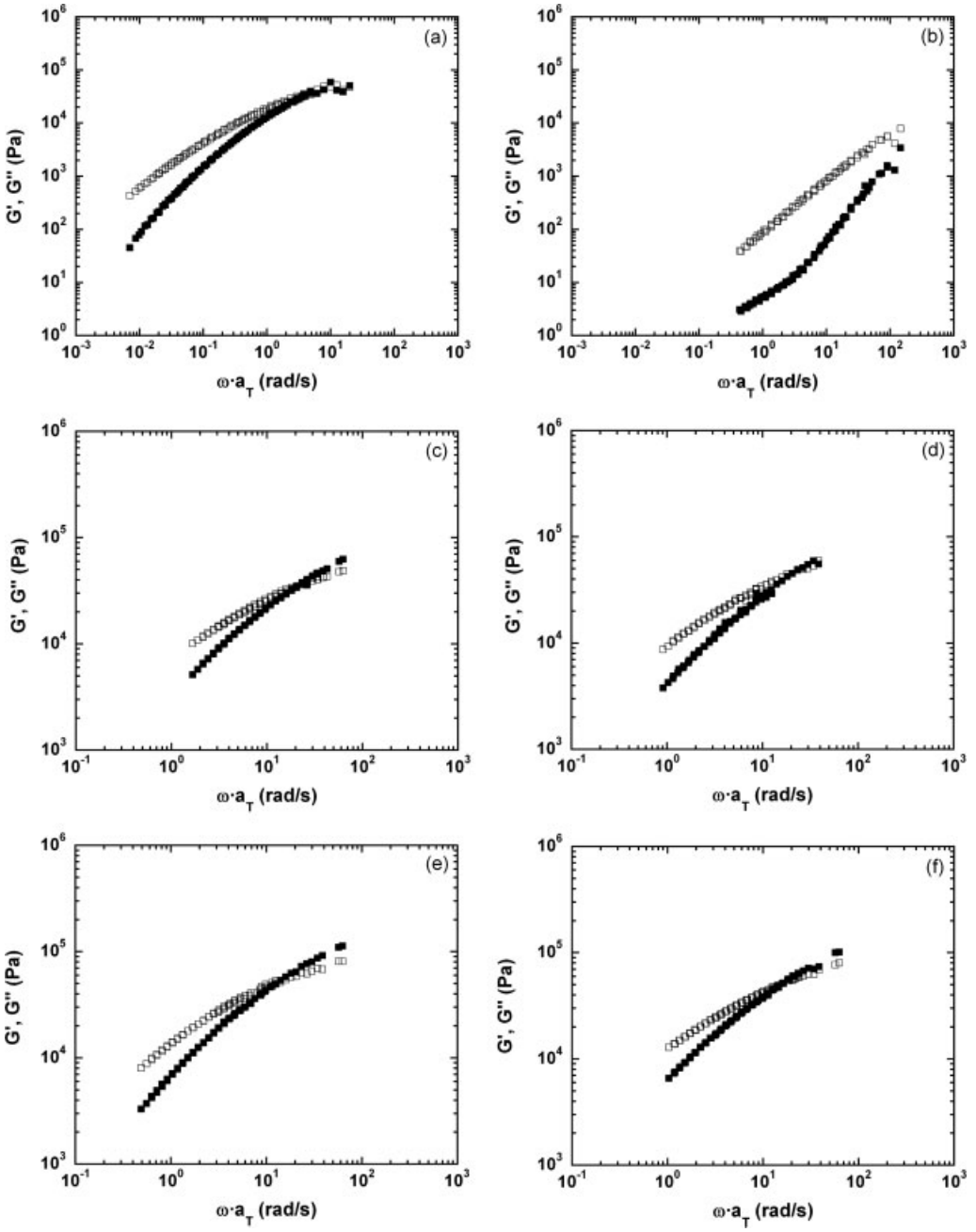

Figure 4 Master curves of dynamic moduli $G'(\omega)$ (filled symbols), and $G''(\omega)$ (open symbols) for (a) iPP and (b) PP-gMA. (c–e) Master curves of 10, 20, and 30 wt % iPP-PAn-SGF, composites; and (f) iPP/PP-gMA with 30 wt % PAn-SGF. T_r = 190°C.

rheological characterization of the polymer and its composites in the linear regime was carried out between 0.002 and 0.004% strains. The dynamic moduli within the LVE regime were characterized by frequency sweeps performed in a range of temperatures from 190 to 230°C.

Time–temperature-superposition

Logarithmic plots of $G'(\omega)$ and $G''(\omega)$ taken at temperature T were superimposed on those for temperature T_r by a translation of *log* a_T along the frequency axis. No shifts along the modulus axis were required. Time-temperature reduction such as this can be expressed by[29]

$$G^{\#}(\omega, T) = G^{\#}(\omega \cdot a_T, T_r,) \quad (1)$$

where the symbol (#) stands for either one prime (′) or two primes (″). In this study we chose a reference temperature, T_r, of 190°C. Figure 4(a) shows the master curve for storage, $G'(\omega)$ and loss, $G''(\omega)$ mod-

TABLE II
Rheological Properties of the Composites, T_r = 190°C

	Oscillation			Steady shear	Creep (t_f^1 = 10s)
Sample	η_0[a] (Pa s)	A_G (Pa s^2)	E_η (kJ/mol)	η_0[b] (Pa s)	$J_e^0 \times 10^{-5}$ (Pa^{-1})
PP0000	11,500	7.62×10^4	51	2335	4.49
PP0010	11,510	4.30×10^3	31	11,360	3.58
PP0020	20,970	1.07×10^4	61	–	2.08
PP0030	24,850	2.14×10^4	79	–	2.83
PP0530	25,320	1.35×10^4	54	–	1.49
PP-gMA	90	–	31	90	–

[a] η_0 from Eq. (4).
[b] η_0 from steady shear.

uli as a function of frequency, ω, for the homopolymer iPP; Figure 4(b) shows the corresponding master curve for PP-gMA. iPP shows a predominantly viscous behavior ($G'(\omega) < G''(\omega)$) at low strain rates and a transition towards the rubber-like regime ($G'(\omega) > G''(\omega)$) as the strain rate increases. On the other hand, the copolymer PP-gMA shows only a predominantly viscous behavior and much smaller moduli values.

The results showed that the composites also obeyed the time–temperature superposition principle. Figures 4(c–e) show the master curves for the iPP-PAn-SGF composites, and Figure 4(f) for the composite of PP-gMA with 30 wt % PAn-SGF. The iPP composites exhibit at low frequencies a predominantly viscous behavior ($G'(\omega) < G''(\omega)$) followed by the rubber-like behavior at high frequencies ($G'(\omega) > G''(\omega)$). It is seen that the PAn-coated glass fibers enhance the elastic behavior of the composites, the shear moduli increase gradually as concentration of filler increases and the terminal regime is significantly reduced. The same sort of behavior is observed for the addition of PAn-SGF filler to the PP-gMA matrix. The 30 wt % composite based on iPP/PP-gMA showed a significant increment in viscous and elastic shear moduli with respect to the iPP matrix. The master curve shown in Figure 4(f) now shows an elastic behavior, as indicated by the dynamic shear moduli behavior, and this is also reflected in the creep recovery behavior, as will be discussed in the following sections.

Over the range of temperatures investigated we found that the TTS shift factors follow an Arrhenius form

$$a_T = \eta(T)/\eta(T_r) \propto e^{E_\eta/RT}, \tag{2}$$

where T is the absolute temperature, R the ideal gas constant, and E_h is the viscosity activation energy. The flow activation energies, E_η, that results from the shift factors are given in Table II. The results show that the addition of PAn-SGF increased the activation energy of the composites. The composite with 30 wt % PAn-coated-SGF exhibits higher flow activation energy of 79 KJ/mol. On the other hand, the addition of PP-gMA decreased the activation energy to 54 KJ/mol for the composite with 30 wt % PAn-SGF.

The dynamic viscosity, $\eta^*(\omega)$, was obtained from the following expression

$$\eta^* = \frac{\sqrt{G'(\omega)^2 + G''(\omega)^2}}{\omega}, \tag{3}$$

Figure 5 shows the dynamic viscosity, $\eta^*(\omega)$, as a function of frequency, ω, for PP-gMA, iPP, and the PAn-coated SGF composites. It can be seen that the complex viscosity increases as the PAn-SGF concentration increases. The increase in complex viscosity for the iPP composites (Fig. 5) is more than double (at 30 wt % concentration of fibers) relative to the neat iPP. On the other hand, it is noticed that the dynamic viscosity of the 30 wt % composites are practically the same over the strain rate range investigated, regardless of the nature of the polymer matrix (iPP versus PP-gMA). We will use $\eta^*(\omega)$ to com-

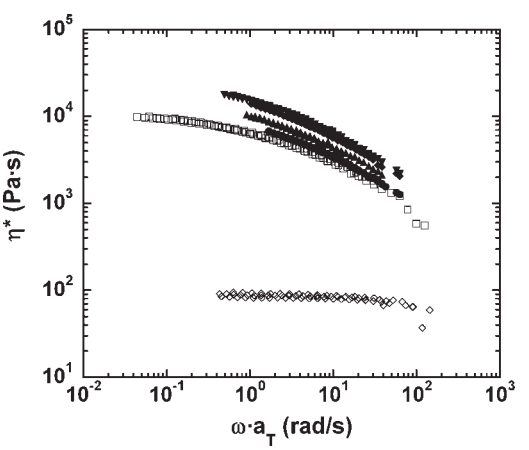

Figure 5 Dynamic viscosity, $\eta^*(\omega)$, as a function of shifted frequency, $\omega \cdot a_T$, for iPP containing: 0 (□), 10 (●), 20 (▲) and 30 (▼) wt % PAn-SGF; and iPP/PP-gMA with 30 wt % PAn-SGF (◆); and for PP-gMA (◇); T_r = 190°C.

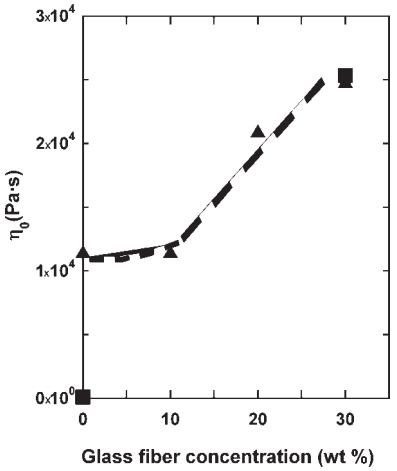

Figure 6 The zero-shear viscosity, η_0, as a function of glass fiber content for the composites with PAn-SGF (▲) and for the composite with PP-gMA (■).

pare the oscillatory flow behavior to the steady shear viscosity, $\eta(\dot{\gamma})$ in the next section.

Behavior in the terminal zone

The rheological behavior of the polymeric melts in the long time region, or terminal zone, were characterized by such parameters as the zero-shear viscosity, $\eta_{0,}$ and elasticity coefficient A_G, which are defined as[29]

$$\eta_\circ = \lim_{\omega \to 0} \frac{G''(\omega)}{\omega} \tag{4}$$

$$A_G = \lim_{\omega \to 0} \frac{G'(\omega)}{\omega^2} \tag{5}$$

The zero-shear viscosity values, η_o, were obtained by fitting the complex viscosity using the Carreau model.[30] Figure 6 shows the values of η_0 as a function of glass fiber concentration; the results show that the composite's η_0 increases gradually with respect to the matrix as the PAn-SGF concentration increases (the broken line is only intended as an eye guide). Again, it is pointed out that the η_0 values of the 30 wt % composites prepared with iPP and PP-gMA are practically the same. In the same manner, it was found that the elasticity coefficients, A_G, also increased as the concentration of PAn-SGF increased. The η_0 and A_G values are listed in Table II. We further explored the elastic behavior of the polymer melts and their composites by studying the flow under creep and monitored the strain recovery.

Effect of temperature

The influence of temperature on possible morphological changes in these composites, such as crystallization, was investigated indirectly by plotting the linear viscoelastic data as log $G'(\omega)$ versus log $G''(\omega)$, a technique that has proven to be useful in the case of linear polymeric chains and block copolymers.[31,32] Results are shown in Figure 7. We observed that the data for all the composites fall on a continuous curve, indicating that no morphological changes occur in the range of temperatures investigated.[31,32] The slopes corresponding to the linear (terminal) region in each plot are (a) 1.26; (b) 1.25; (c) 1.45; (d) 1.46; (e) 1.36; and (f) 1.42.

Steady shear

We also investigated the steady shear flow behavior of the composites. Figure 8 shows the steady shear viscosity, η, as a function of shear rate, $\dot{\gamma}$, for the neat polymers and their composites. The viscosity of the molten iPP shows a Newtonian behavior up to about 1 s^{-1} shear rate, and then becomes shear thinning. On the other hand, the viscosity of 10 wt % PAn-SGF composite showed a significant increase with respect to the matrix, almost fivefold at shear rates lower than 0.1 s^{-1}. However, increasing the shear rate the viscosity rapidly became shear thinning and at higher shear rates (>3 s^{-1}) the melt viscosity of the composite matched and eventually fell below that of the polymer matrix.

The melt viscosity of the 20 wt % iPP-PAn-SGF composite showed a rather intriguing behavior, at lower shear rates the viscosity was significantly smaller than that of the 10 wt % composite but still larger than the matrix's viscosity. The viscosity also showed a shear-thinning behavior at all shear rates and increasing the shear rate above 0.2 s^{-1} the viscosity rapidly fell below the iPP's viscosity. Then, increasing the concentration of filler at 30 wt % we can see an increase of melt viscosity with respect to the 20 wt % composite, but the viscosity values were still lower than the 10 wt % composite. The melt viscosity of the 30 wt % composite also behave shear thinning and at higher shear rates (>1 s^{-1}) the viscosity values also fell below the matrix's viscosity values.

The melt viscosity of PP-gMA showed a predominantly Newtonian behavior up to about 7 s^{-1} shear rate and a Newtonian viscosity of about 90 Pa s. The melt viscosity of the iPP/PP-gMA composite showed significant shear thinning behavior, changing from $\sim$ 10,000 Pa s at 0.1 s^{-1} to $\sim$ 300 Pa s at 10 s^{-1}. The low shear rate behavior also suggests the presence of a yield stress.

The Carreau model[30] was used to obtain the zero-shear viscosities, η_0, by fitting the viscosity data, η, as a function of shear rate, $\dot{\gamma}$. Table II shows the values of η_0 for iPP containing 0 and 10 wt % PAn-SGF and for PP-gMA containing composite. The compos-

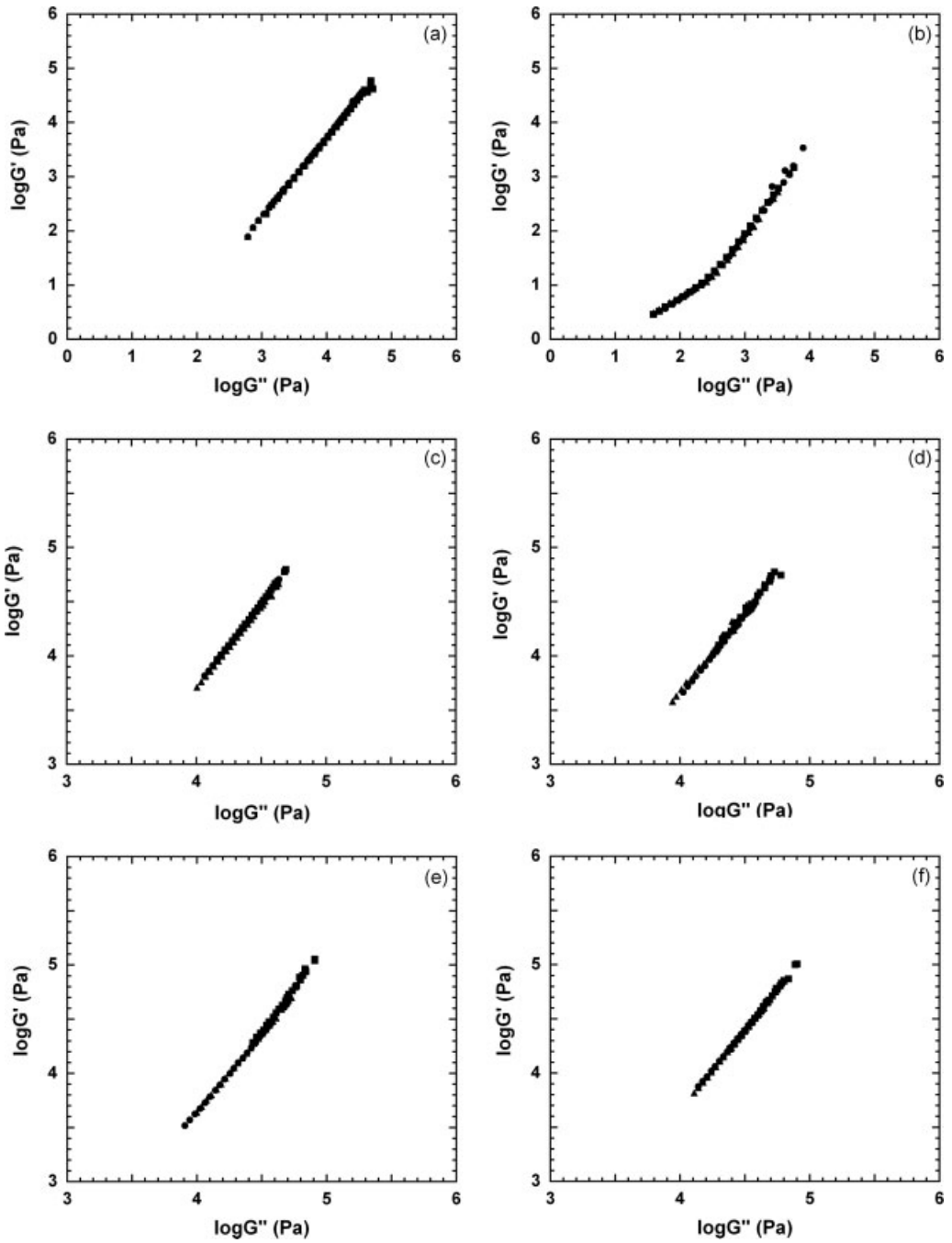

Figure 7 Log $G'(\omega)$ as a function of Log $G''(\omega)$ for iPP (a) and PP-gMA (b). (c–e) iPP containing: 10, 20, and 30 wt % PAn-SGF, respectively; and (f) iPP/PP-gMA with 30 wt % PAn-SGF. At 190 (■), 210 (●), and 230 (▲) °C. The slopes corresponding to the linear (terminal) region in each plot are (a) 1.26; (b) 1.25; (c) 1.45; (d) 1.46; (e) 1.36; and (f) 1.42.

ite with 10 wt % PAn-SGF increased the zero-shear viscosity from 2335 to 11360 Pa s. We can see that the empirical Cox-Merz rule,[33] which states that $\eta^*(\omega) = \eta(\dot{\gamma})$ for $\omega = \dot{\gamma}$, and is typically applicable for homopolymers, fails for the case of composites with 20 and 30 wt % PAn-SGF and for the PP-gMA containing composite.

However, the results showing first the rising and then lowering of steady shear viscosity as concentration of filler increased obtained for the iPP-PAn-SGF composites are rather unexpected. It is suggested that shear flow may induce disorder of the fibers at lower concentration, whereas at higher fiber concentration there may be a flow-induced alignment of the fibers, in the same manner as the isotropic-nematic transition of liquid crystalline polymers[34] and carbon nanotubes dispersions.[35] To explore this hypothesis we carried out rheo-optical experiments on these composites, these are discussed in the following section.

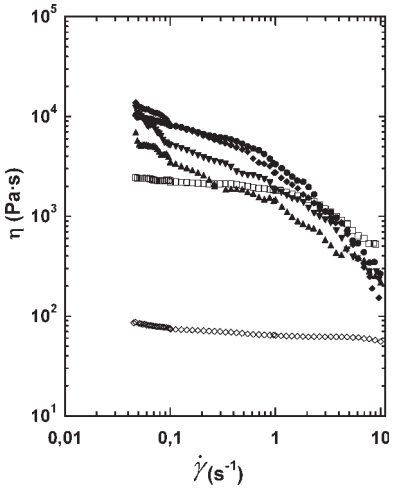

Figure 8 Steady shear viscosity, η, as a fuction of shear rate, $\dot{\gamma}$, for iPP containing: 0 (□), 10 (●), 20 (▲) and 30 (▼) wt % PAn-SGF; and iPP/PP-gMA with 30 wt % PAn-SGF (◆); and for PP-gMA (◇); T_r = 190°C.

Rheo-optics

The influence of shear flow on microfiber alignment was investigated *in situ*, by applying shear to the molten composite containing 10 wt % PAn-SGF. Figure 9 shows a series of micrographs obtained at 190°C while applying shear at a nominal rate of 0.5 s^{-1}. It is at this shear rate where we observed larger differences between the melt viscosity of the matrix and the composites (see Fig. 8). The arrow in Figure 9(a) indicates the shear flow axis. Figure 9(b-d) shows that within the first 10 s of shearing there is little change in the initial microfiber orientation. However, after 20 s of continuous shearing the results showed that shear has induced disorientation

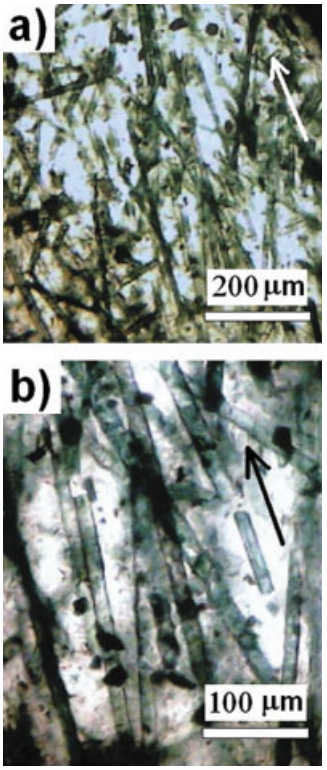

Figure 10 Micrograph of iPP composite with 20 wt % PAn-SGF after shearing for 30 s at a shear rate of $\dot{\gamma}$ = 0.5 s^{-1} and 190°C. White light conditions. [Color figure can be viewed in the online issue, which is available at www. interscience.wiley.com.]

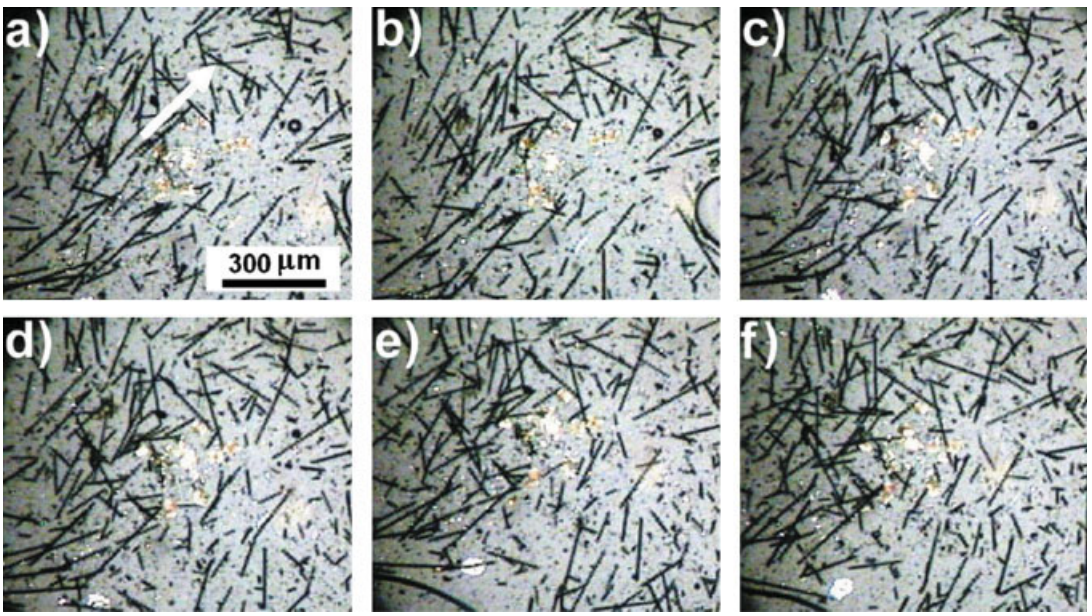

Figure 9 Micrographs of iPP composite with 10 wt % PAn-SGF under steady shear at a shear rate of $\dot{\gamma}$ = 0.5 s^{-1} and 190°C. Micrographs obtained after (a) 0, (b) 2, (c) 4, (d) 10, (e) 20, and (f) 30 s after shear started. White light conditions. [Color figure can be viewed in the online issue, which is available at www.interscience.wiley.com.]

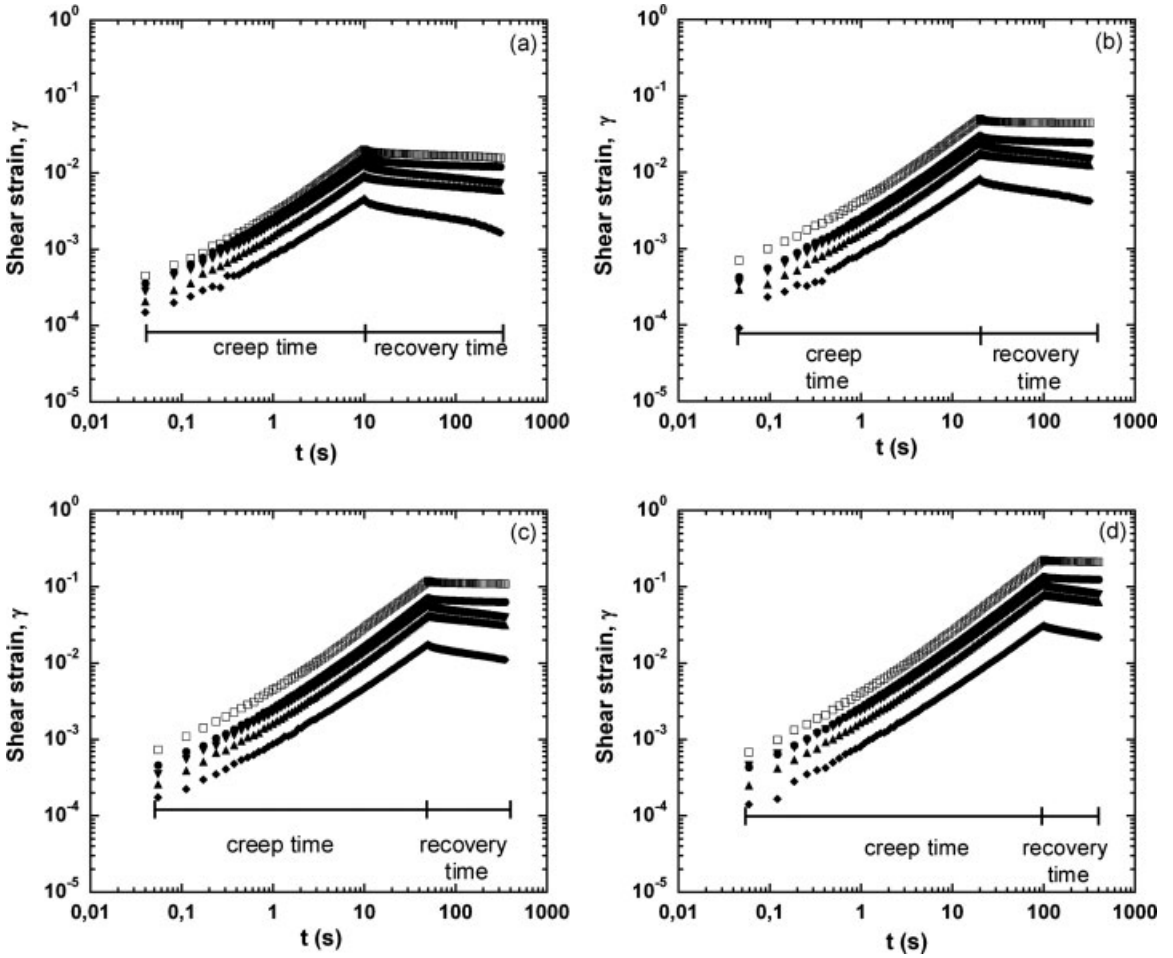

Figure 11 Shear strain, γ, for iPP containing: 0 (□), 10 (●), 20 (▲) and 30 (▼) wt % PAn-SGF; and iPP/PP-gMA with 30 wt % PAn-SGF GF (◆). During creep time period of (a)–(d), t_f^1 = 10, 20, 50, and 100 s, respectively, T_r = 190°C.

of the microfibers [Fig. 9(e)]. This disorientation is even more marked as shearing continuous [Fig. 9(f)].

The influence of shear flow on composites of higher filler concentration is quite different. Figure 10 shows a micrograph of a 20 wt % PAn-SGF composite after being subjected to 0.5 s^{-1} shear rate at 190°C and for 30 s. The micrograph shows clearly that shear has induced significant microfiber alignment along the flow direction.

The rheo-optical results would then explain the steady shear viscosity behavior shown in Figure 8. However, more investigation is being carried out on the influence of shear flow on fiber orientation in these composites and will be the subject of a future publication.

Creep

In a shear creep recovery experiment, a constant shear stress, σ, of 10 Pa was applied to the iPP composites and the resultant deformation measured as a function of time. These experiments were carried out at 190°C. The influence of the creep time and the creep time recovery on the time dependent strain, γ(*t*), is demonstrated in Figure 11(a–d). It can be seen that the strain deformation increased as the creep time increased. We can observe that the addition of PAn-SGF decreased the strain deformation. For all creep time considered, the neat iPP showed the largest strain deformation and the smallest strain recovery. On the other hand, investigating the behavior of PP-gMA containing composite showed the smallest strain deformation.

After creep time the stress is removed and there is a strain recovery process (memory effect) based on the melt elasticity of the material. Special emphasis is put on the percentage of recoverable strain, γ_R. The total recoverable strain normalized with respect to the applied stress, is referred to as the shear compliance $J_e^0 = \gamma_R/\sigma$.[29] In Table II we can see that the shear compliance, J_e^0, decreased as the concentration of PAn-SGF increased.

As stated above, the total recoverable strain is a measurement of the material's elasticity, i.e., the mechanical energy stored in the sample during the creep stage. Figure 12 shows the percentage of

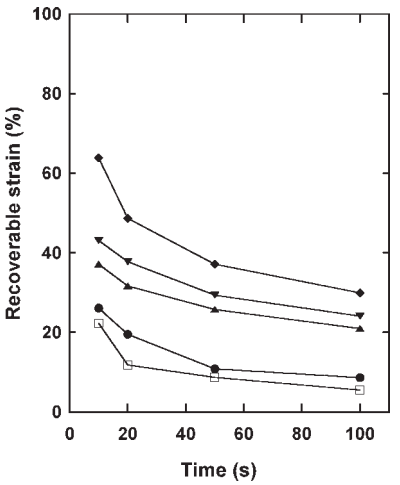

Figure 12 Percentage of recoverable strain, $\gamma_R[=\gamma(t_f^2)/\gamma(t_f^1) \times 100]$, as a function of creep time for iPP containing: 0 (□), 10 (●), 20 (▲) and 30 (▼) wt % PAn-SGF; and iPP/PP-gMA with 30 wt % PAn-SGF (◆); T_r = 190°C.

recoverable strain, γ_R, as a function of creep time. γ_R is defined as follows

$$\gamma_R = \frac{\gamma(t_f^2)}{\gamma(t_f^1)} \times 100 \quad (6)$$

where t_f^1 is the time elapsed during applied stress and t_f^2 is the time allowed for strain recovery. For all samples the increase in creep time diminished the percentage of recoverable strain, γ_R. However, we can also observe that the addition of PAn-SGF increased the recoverable strain (and melt elasticity) of iPP-based composites. However, the composite based on the blend iPP/PP-gMA showed the largest recoverable strain of all composites. For instance, at a creep time of t_f^1 = 10 s, the iPP/PP-gMA based composite with 30 wt % PAn-SGF has a recoverable strain, γ_R, of 64%, whereas the iPP-based composite with 30 wt % PAn-SGF has a recoverable strain of only 43%.

CONCLUSIONS

The results of this investigation have shown that the reinforcement of iPP with PAn-coated-SGF lead to an increase of the melt elasticity as measured by the recoverable strain of the composite. As the concentration of the filler increased, the dynamic moduli increased correspondingly. This is important for the preparation of resistant composites with a relatively good electrical conductivity, arising from the PAn conductivity, which can be used for antistatic purposes. Although the dynamic viscosity η^* of the iPP composites also increased as the filler concentration increased, the steady state viscosity η showed interesting results. First η increased and then decreased as the filler concentration changed from 10 to 20 wt %. Finally, the steady state viscosity increased again at the concentration of 30 wt %. The decrease in steady state viscosity would be useful in the easiness of the preparation of the composites by, say, extrusion processing. Based on rheo-optical results, the anomalous steady state viscosity behavior of the iPP/PAn-SGF composites was explained by the flow-induced disorder and alignment of the fibers. Finally, the composite based on the iPP/PP-gMA blend showed the largest increment in melt viscosity and recoverable strain, suggesting better adhesion between the matrix and the PAn-SGF filler, in agreement with mechanical analysis results.[16]

M. E. Romero-Guzmán was supported by a postdoctoral fellowship from DGAPA-UNAM.

References

1. Gupta, A. K.; Purwar, S. N. J Appl Polym Sci 1986, 31, 535.
2. Bassani, A.; Pessan, L. A.; Hage E. J Appl Polym Sci 2001, 82, 2153.
3. Setz, S.; Stricker, F.; Kressler, J.; Duscher, T.; Mulhaupt, R. J Appl Polym Sci 1996, 59, 117.
4. Veenstra, H.; van Lent, B. J.; van Dam, J.; de Boer, A. P. Polymer 1999, 40, 6661.
5. Kucera, J.; Nezbedova, E. Polym Adv Technol 2007, 18, 112.
6. Varatharajan, R.; Malhotra, S. K.; Vijayaraghavan, L.; Krishnamurthy, R. Mater Sci Eng B 2006, 132, 134.
7. Panthapulakkal, S.; Sain, M. J Appl Polym Sci 2007, 103, 2432.
8. Kumar, K. S.; Bhatnagar, N.; Ghosh, A. K. J Reinforc Plast Compos 2007, 26, 239.
9. Greene, J. P.; Wilkes, J. O. Polym Eng Sci 1995, 35, 1670.
10. Bush, S. F.; Torres, F. G.; Methven, J. M. Compos A 2000, 31, 1421.
11. Xie, H. Q.; Zhang, S.; Xie, D. J Appl Polym Sci 2005, 96, 1414.
12. Ausias, G.; Agassant, J. F.; Vincent, M.; Lafleur, P. G.; Lavoie, P. A.; Carreau, P. J. J Rheol 1992, 36, 525.
13. Beauline, M.; Mitsoulis, E. J Reinforc Plast Compos 2003, 22, 1625.
14. Sepehr, M.; Ausias, G.; Carreau, P. J. J Non-Newtonian Fluid Mech 2004, 123, 19.
15. Cruz-Silva, R.; Romero-García, J.; Angulo-Sánchez, J. L. Mater Sci 2005, 40, 5107.
16. Cruz-Silva, R.; Romero-García, J.; Vazquez-Rodriguez, S.; Angulo-Sánchez, J. L. J Appl Polym Sci 2007, 105, 2387.
17. Taipalus, R.; Harmia, T.; Friedrich, K. Appl Compos Mater 1999, 6, 167.
18. Jia, W.; Tchoudakov, R.; Segal, E.; Narkis, M.; Siegmann, A. J Appl Polym Sci 2004, 91, 1329.
19. Faez, R.; Martin, I. M.; de Paoli M.-A.; Rezende M. C. J Appl Polym Sci 2002, 83, 1568.
20. Taipalus, R.; Harmia, T.; Friedrich, K. Polym Compos 2000, 21, 396.
21. Flandin, L.; Bidan, G.; Brechet, Y.; Cavaillé, J. Y. Polym Compos 2000, 21, 165.
22. Jia, W.; Tchoudakov, R.; Segal, E.; Joseph, R.; Narkis, M.; Siegmann, A. Synth Met 2003, 132, 269.

23. Barra, G. M. O.; Jacques, L. B.; Oréfice, R. L.; Carneiro, J. R. G. Eur Polym Mater 2004, 40, 2017.
24. Macdiarmid, A. G. Curr Appl Phys 2001, 1, 269.
25. Li, Z. F.; Ruckenstein, E. Synth Met 2002, 129, 73.
26. Marrucci, G.; Grizzuti, N.; Buonaurio, A. Mol Cryst Liq Cryst 1987, 153, 263.
27. Bedford, S. E.; Windle, A. H. Polymer 1990, 31, 616.
28. Marsano, E.; Carpaneto, L.; Ciferri, A. Mol Cryst Liq Cryst 1988, 158B, 267.
29. Ferry, J. D. Viscoelastic Properties of Polymers, 3rd ed.; Wiley: New York, 1980.
30. Carreau, P. J. J Rheol 1972, 16, 99.
31. Han, C. D.; Kim, J. J Polym Sci Part B: Polym Phys 1987, 25, 1741.
32. Han, C. D.; Jhon, M. S. J Appl Polym Sci 1986, 32, 3809.
33. Cox, W. P.; Merz, E. H. J Polym Sci 1958, 28, 619.
34. Donald, A. M.; Windle, A. H. Liquid Crystalline Polymers; Cambridge University Press: Cambridge, 1992.
35. Song, W.; Kinloch, I. A.; Windle, A. H. Science 2003, 302, 1363.